Published in final edited form as:
Ann N Y Acad Sci. 2010 March ; 1192(1): 95–102. doi:10.1111/j.1749-6632.2009.05376.x.

Noninvasive methods of measuring bone blood perfusion

J.P. Dyke[1] and **R.K. Aaron**[2]

[1]Citigroup Biomedical Imaging Center, Department of Radiology, Weill Medical College of Cornell University, New York, New York, USA

[2]Department of Orthopaedics, Warren Alpert Medical School of Brown University, Providence, Rhode Island, USA

Abstract

Measurement of bone blood flow and perfusion characteristics in a noninvasive and serial manner would be advantageous in assessing revascularization after trauma and the possible risk of avascular necrosis. Many disease states, including osteoporosis, osteoarthritis, and bone neoplasms, result in disturbed bone perfusion. A causal link between bone perfusion and remodeling has shown its importance in sustained healing and regrowth following injury. Measurement of perfusion and permeability within the bone was performed with small and macromolecular contrast media, using dynamic contrast-enhanced magnetic resonance imaging in models of osteoarthritis and the femoral head. Bone blood flow and remodeling was estimated using ^{18}F-Fluoride positron emission tomography in fracture healing and osteoarthritis. Multimodality assessment of bone blood flow, permeability, and remodeling by using noninvasive imaging techniques may provide information essential in monitoring subsequent rates of healing and response to treatment as well as identifying candidates for additional therapeutic or surgical interventions.

Keywords

DCE-MRI; ^{18}F-Fluoride PET; bone perfusion; fracture healing; osteoarthritis

Introduction

The ability to quantitatively measure blood flow in bone noninvasively and repeatedly would be of great importance in a wide variety of skeletal conditions, including trauma, infection, inflammation, arthritis, avascular necrosis neoplasms, and bone grafting. The inception of novel noninvasive imaging techniques using injection of various contrast agents has provided glimpses of methods to assess bone perfusion in the clinical setting. Specifically, in this article we will discuss acquisition and analysis methods of estimating bone perfusion using various contrast agents in magnetic resonance imaging (MRI) and positron emission tomography (PET).

Perfusion assesses blood flow at the level of the capillary bed within tissue. Measurement of blood flow within larger arterial and venous beds is accomplished routinely in the clinic using various angiographic imaging techniques. While digital subtraction angiography allows for

Address for correspondence: Jonathan P. Dyke, Ph.D., Assistant Research Professor of Physics, Radiology, Citigroup Biomedical Imaging Center, Weill Cornell Medical College, 1300 York Avenue – Box 234, New York, NY 10021. jpd2001@med.cornell.edu.

Conflict of interest

The authors declare no conflicts of interest.

discrimination of sub-millimeter vessel diameters, tissue perfusion occurs on the scale of 5–10 μm within the capillary bed. In addition, identification of various feeding vessels in soft tissue structures within the body may be readily done with the aid of contrast-enhanced imaging techniques. However, quantitation of bone blood flow is confounded by the sheer density of bone itself in addition to the heterogeneity of blood supply within the osseous structures.[1]

As in other tissues, adequate regulation of bone perfusion is essential in insuring proper levels of oxygenation, delivery of nutrients, as well as elimination of waste.[2] Within bone there is a known synergism between bone blood flow and remodeling, which is crucial for subsequent healing to occur. Bone neovascularization is thought to play a significant role in the healing process following fracture, joint replacement, and bone grafts. Reduced perfusion as related to bone remodeling is causally related to an increased risk of fracture.[3] Noninvasive serial assessment of perfusion would yield information pertinent to the rate of healing and risk of avascular necrosis. Perfusion data may also be of use in identifying candidates for joint replacement and additional surgical intervention. Novel bone morphogenic proteins, growth hormones, and cytokines offer benefits for patients requiring stimulated healing. Clinical decision making would benefit from identifying patients known to have adequate regional perfusion to obtain the greatest distribution and outcome benefit from these agents.

The clinical relevance of assessing bone blood flow is seen in the large number of disease states that present with an etiology of bone perfusion disturbances. Reduced bone blood perfusion is also an indicator of disease progression and severity. One example of this is the cascading morbidity resulting from tobacco smoking and the resulting decreased bone perfusion and oxygenation compared to nonsmokers. 4 The effect of reduced bone blood flow resulted in a decreased rate of bone remodeling and increased risk of osteoporosis in smokers. Similarly, there is a reported link between decreased bone perfusion and osteoporosis.[5] The resulting decrease in bone mineral density (BMD) was mirrored by an increase in fatty marrow and decreased perfusion.

The progression of osteoarthritis (OA) is characterized by the interaction of various metabolic, genetic, biochemical, and biomechanical processes and cannot be simply defined by a single imaging parameter. The role of vascular disturbances in the etiology of osteoarthritis is known to causally interact with changes in intraosseous pressure, capillary permeability, cartilage volume and structure, and bone remodeling. Our work suggests that a decrease in bone perfusion may be related to venous outflow obstruction in a preclinical model of OA.[6] Knowledge of bone blood flow and turnover may be of potential utility for identifying future mechanisms and targets of various tailored drugs in the treatment of OA.

Assessment of tumor perfusion is essential in not only determining the angiogenic progression of the lesion but also in estimating adequate drug delivery of various chemotherapy regimens. Tumors activate certain gene signaling pathways to stimulate new vessel growth. Oxygen and nutrientsmay diffuse approximately 160 μm beyond the feeding vessel. Tumor growth beyond a diameter of 2–3 mm without adequate tissue perfusion results in hypoxia. This role of perfusion in tumor growth has led to the development of the class of anti-angiogenic drugs in use today.

Magnetic resonance imaging

A primary strength of MRI lies in its ability to provide variable soft tissue contrast related to the inherent T_1 and T_2 relaxivities of the tissue. Traditional MRI of osseous substructures yields excellent detail of both cortical and trabecular bone.[7] The incorporation of contrast media into an MRI study allows assessment of angiogenic activity as well as estimation of physiological parameters, such as permeability, blood flow, and clearance rates. The independent extraction

of these parameters relies on the size and binding affinities of the contrast media used and will be broken into small (SMCM) and macro(MMCM) molecular contrast media.

Small molecular contrast media

With the introduction of the first gadolinium (Gd)-based MR contrast agent to the clinical community in 1988, the necessity of contrast-enhanced MRI has arisen in the study of oncology, infection, inflammation, stroke, and vascular abnormalities. Contrast-enhanced agents have a molecular weight of approximately 538 Da, with a clearance time of 12 min in the plasma space for individuals with normal (>30 mL/min/1.73 m^2) renal function (e.g., Gd-diethylenetriaminopentaacetic acid [DTPA]). The contrast media remains extracellular and does not cross the intact blood–brain barrier; it may be used to assess a combination of blood flow and permeability in tissues.

Uptake of SMCM in bone has been evaluated using dynamic contrast-enhanced MRI (DCE-MRI) techniques. In our studies, we have assessed contrast uptake in the Dunkin-Hartley guinea pig model of OA as well as in clinical studies of bone marrow lesions.8 We hypothesized that changes in fluid dynamics in subchondral bone bore a functional relationship to bone remodeling and cartilage breakdown in OA. Animals of four different ages (6, 9, 12, and 15 months) representing various stages in the development of OA were studied. All animals underwent DCE-MRI, and perfusion data were analyzed based on the Brix pharmacokinetic model.9 Regions of interest (ROIs) at the medial and lateral tibial plateaus (Fig. 1)were compared to histological Mankin scores of articular cartilage and subchondral bone plate thickness. A decrease in perfusion was observed in animals between 6 and 9 months of age in the medial tibial plateau. These changes temporally preceded the morphologic changes of OA in cartilage and bone.[10] The eventual cartilage and bone lesions of OA occurred in the medial tibia and were later seen in the lateral tibia once OA lesions were established. DCE-MRI can extract kinetic information on bone perfusion in an animal model of OA. Signal enhancement in subchondral bone temporally preceded and spatially localized at the same site of the eventual bone and cartilage lesions, suggesting venous outflow obstruction as an underlying mechanism.

A correlation has been proposed between reduced bone perfusion and decreased BMD, strengthening the causal link between bone blood flow and remodeling.[11] MRI-derived indices of bone perfusion using DCE-MRI showed reduced perfusion in the femoral head and neck in patients with decreased BMD and osteoporosis compared to those with normal levels of perfusion. Additional studies by our group assessed perfusion of the cadaveric femoral head (Fig. S1) with and without ligation of the medial circumflex femoral artery by using Gd-DTPA MRI and validated the results via polyurethane injections and gross dissection.[12] Quantitation of bone perfusion using static post-contrast MRI yielded the percentage enhancement of the femoral head by specific feeding vessels. This is of clinical interest in assessing the ability of the head to reperfuse and the resulting risk of necrosis following vascular damage after fracture of the femoral neck. Contrast-enhanced MRI shows the potential to assess bone blood flow in various disease and injury states, which is essential in estimating the risk of avascular necrosis and subsequent rates of healing.

Supporting Information

Additional supporting information may be found in the online version of this article:

Figure S1. Sagittal, postcontrast, fat-suppressed MRI of the cadaveric femoral head showing uptake in the (**A**) side having a ligated medial circumflex femoral artery (MFCA) and (**B**) control nonligated side. Perfusion of the femoral head was shown to occur from anastamosis and delivery of contrast through the lesser venous branches.

Figure S2. A generalized compartmental model is shown illustrating the permeability surface area product (K_{trans}) between the plasma (v_p) and extravascular extracellular space (v_e).

Figure S3. Analysis of ^{18}F-Fluoride positron emission tomography data is based on this three-compartment model described by Hawkins *et al.*[19]

Please note: Wiley–Blackwell are not responsible for the content or functionality of any supporting materials supplied by the authors. Any queries (other than missing material) should be directed to the corresponding author for the article.

Quantitative assessment of SMCM MRI techniques

A T_1-weighted DCE-MRI time-intensity curve displays MR signal intensity as a function of time for each voxel in the image following administration of contrast (i.e., Fig. 1). Although qualitative measurements may be made of initial slope, area under the curve, and percentage enhancement to characterize inflow of contrast to the region, pharmacokinetic modeling provides amore quantitative link between signal intensity and physiological perfusion parameters in bone. The indicator dilution theory was proposed in 1948 by Kety and Schmidt to describe the freely diffusible movement of a tracer through the vasculature. The conversion from the MR signal intensity to the concentration of the tracer in mmol requires knowledge of the T_1 relaxation time prior to injection. Estimation of the permeability surface area product in tissue (C_t) can be made with knowledge of the plasma input function (C_p) via:

$$C_t(t)=\upsilon_p C_p(t) + C_p(t) \otimes K^{\text{trans}} e^{\frac{-K^{\text{trans}}}{\upsilon_e}}.$$

A generalized compartmental model is shown in Figure S2 that illustrates the permeability surface area product (K_{trans}) between the plasma (υ_p) and extravascular extracellular space (υ_e). Elimination of the tracer from the region (K_{out}, k_{el}) characterizes venous outflow and clearance of the tracer from bone.

Macromolecular contrast media

MMCM have a molecular weight of approximately 92,000 Da, with a clearance time of 3 h (e.g., albumin-$[\text{Gd-DTPA}]_{30}$) in comparison with SMCM. Given the large molecular weight, enhancement in normal tissues having tight endothelial junctions and normal vascular permeability can remain constant for approximately 60 min after injection. The utility of MMCM yields flow-independent estimates of permeability surface area product, plasma volume, and fractional leak rate.[13] SMCM diffuse freely across normal capillary beds and are rapidly cleared. Also, estimates of permeability with SMCM are confounded by reduced rates of blood flow.[14] In the regime where blood flow greatly exceeds the rate of vascular permeability surface area product, then SMCM (K_{trans}) is an estimate of permeability. If blood flow is greatly reduced, then K_{trans} becomes a combination of flow and permeability. However, while MMCM are delivered to all tissues, they will only accumulate in areas with increased vascular permeability, and quantitative measures of permeability are not subject to contributions from flow.

Figure 2 illustrates *in vivo* uptake of albumin-$(\text{Gd-DTPA})_{30}$ (courtesy of University of California, San Francisco, Contrast Media Laboratory) in the tibia of an 18-month-old Dunkin-Hartley guinea pig model of OA in our study. A fast, T_1-weighted, spoiled gradient echo sequence acquired DCE-MRI images of the medial and lateral tibial plateau at a rate of 7.7 sec for a period of 10 min following injection at a concentration of 0.03 mmol/kg. Additional time-intensity curves were plotted for the popliteal artery and tibial diaphysis to show uptake over time. Notice that the level of tissue enhancement had not reached a plateau by the end of the scan. This technique has also detected abnormal synovium in animal models of OA.[16] DCE-MRI, using MMCM agents, holds promise for assessing bone permeability surface area product in regions of increased intraosseous pressure, such as the medial tibial plateau. These estimates may provide information on whether permeability is reduced in bone from increased pressure in advanced states of OA.

Quantitative assessment of MMCM MRI techniques

SMCM require a three-compartment pharmacokinetic model to yield accurate estimates of physiological perfusion parameters. In the case of MMCM, the reflux rate from the

extravascular extracellular space to the plasma space is insignificant.[13] This reduces the system to a two-compartment model that can be solved graphically via methods developed by Patlak.[15] The assumption that the MMCM do not return to the plasma space during the course of the slope of the following equation with a linear regression:[16]

$$\frac{C_t(t)}{C_p(t)} = BV + \frac{PS}{(1 - Hct)} \frac{\int_0^t C_p(\tau) d\tau}{C_p(t)}.$$

The plasma volume (PV) is found as PV = BV (1 − Hct) by fitting the intercept of the equation to the blood volume (BV) and knowing the hematocrit (Hct). The fractional leak rate is also known from the ratio of PS/PV.

Positron emission tomography

PET uses injection of a specific radiotracer to yield quantitative information regarding the localization and metabolic activity of tissues. Traditional oncologic applications of PET use glucose ([18F]fluorodeoxyglucose; [^{18}F-FDG])-based tracers in addition to various radiolabeled amino acids and ligands to concentrate uptake in malignant cell groups. Standard glucose-based compounds (FDG) do not yield a high level of accuracy specific to bone or OA, although the use of FDG may provide information related to inflammation in the synovium and remodeling of intra-articular tissues.[17] However, the chemical precursor to FDG, ^{18}F-Fluoride, (sodium fluoride [NaF]) is a U.S. Food and Drug Administration (FDA)-approved bone-seeking radiotracer that has been known to bind to hydroxyapatite in the bone matrix since sodium floride's inception in the early 1970s.[18] Dynamic PET time-activity curves (TAC) allow differentiation of bone blood flow in the angiogenic phase from bone mineral binding and bone formation in the osteoblastic phase. Specifically, it is assumed that complete extraction of ^{18}F-Fluoride occurs during the first few minutes after injection, allowing for assessment of bone blood flow. At the time of maximal uptake (45–60 min postinjection), the ^{18}F-Fluoride binds to hydroxyapatite in the bone matrix, reflecting bone turnover.

Figure 3 shows work from our group using ^{18}F-Fluoride PET to image the knee in an 18-month-old Dunkin-Hartley guinea pig model of OA. PET studies were acquired on a Siemens/CTI Concorde Focus 220 microPET scanner (Siemens Medical Solutions USA, Inc., Knoxville, TN). ^{18}F-Fluoride was administered through a central venous subcutaneous access port at an activity of 1.4mCi/kg, and data were acquired at 2-sec intervals for 60 min. Frames were fixed at 2-sec intervals for the first 2min to accurately characterize the blood curve and later summed to produce 2-min intervals for the duration of the scan. Representative ^{18}F-Fluoride time-activity curves from the femoral artery and medial/lateral tibial plateaus are shown (Fig. 3).

Figure 4 displays a transverse view and serial dynamic ^{18}F-Fluoride PET time-activity curves from our study placed on a cortical region of a fracture of the distal radius in a human subject. A nonsignificant risk investigational device exemption waiver was obtained from the FDA with regards to acquiring high resolution (1.5 × 1.5 × 1.0 mm) dynamic PET studies on human subjects under care of the Institutional Review Board, using the Siemens/CTI Concorde Focus 220 microPET scanner (Siemens). Attenuation correction was performed using a 122 keV ^{57}Co source in singles mode. As a control, static imaging was acquired from the contralateral distal ulna 50–60 min postinjection. To our knowledge, these preliminary data are the first to serially assess fracture healing using ^{18}F-Fluoride PET imaging techniques.

Positron emission tomography ^{18}F-Fluoride analysis methods

Analysis of ^{18}F-Fluoride PET data is based on the three-compartment model described by Hawkins *et al.* shown in Figure S3. The model consists of the following compartments: plasma

(C_p), extravascular compartment (C_e), and bone (C_b).[19] The forward transfer of ^{18}F-Fluoride from plasma to whole bone (K_1) is related to bone blood flow (BBF) by: K_1=E · BBF · PCV, where PCV is the packed cell volume. This assumes that complete extraction of the tracer (E) occurs during the first few minutes after injection.[20] Estimates of bone blood flow have been published with ^{18}F-Fluoride studies of porcine bone that have been validated with ^{15}O-H_2O PET.[21,22] The assumption in this analysis is that a fixed permeability of bone is present. Possible incorporation of multimodality DCE-MRI estimates of permeability surface area product would provide insight into this assumption within different osseous structures.

Following rapid clearance of ^{18}F-Fluoride from the plasma, the fluoride exchanges ions with the hydroxyl group in the hydroxyapatite crystal of bone to form fluoroapatite.[19] The net uptake of fluoride to the bone mineral compartment, known as the net fluoride influx rate, is calculated as: $K_i = K_1k_3/(k_2 + k_3)$. Graphical analysis may be performed using the Patlak method[15] to yield K_{pat}, which has been shown to significantly correlate with the net influx rate K_i. This influx rate of fluoride to bone is indicative of the level of bone remodeling and mineralization and provides complementary information to estimates of bone blood flow.

Conclusions

There is a complex physicochemical environment present within regions of bone. Interactions can exist between any number of the following processes: venous stasis, intraosseous hypertension, bone blood flow (perfusion), hypoxia, and acidosis. Noninvasive imaging techniques, such as MRI and PET, have been developed that allow us to gain insight into spatially varying regions of capillary permeability, bone blood flow, and remodeling within various regions of bone. Independent multimodality measurement of these parameters may allow patient-specific assessment of bone perfusion that is essential in all aspects of healing and possibly causal in proper bone remodeling. Serial monitoring of perfusion abnormalities in bone may identify patients at risk for avascular necrosis or delayed healing. These techniques may also allow for serial monitoring of bone perfusion in response to treatment.

Acknowledgments

J.P.D. acknowledges funding from the Clinical and Translational Science Center at Weill Cornell Medical College supported by UL1RR024996/National Institutes of Health (NIH). R.K.A. and J.P.D. acknowledge support of AstraZeneca, U.K., and R.K.A. acknowledges support from NIH AR 2K24AR002128-06A2.

References

1. McCarthy I. The physiology of bone blood flow: a review. J. Bone Joint Surg. Am 2006;88:4–9. [PubMed: 17079361]
2. Dyke, JP. Perfusion imaging. In: Holodny, AI., editor. Perfusion Imaging. Functional Neuroimaging: A Clinical Approach. Informa Healthcare; 2008. p. 249-272.
3. Wang YX, Griffith JF, Kwok AW, et al. Reduced bone perfusion in proximal femur of subjects with decreased bone mineral density preferentially affects the femoral neck. Bone 2009;45:711–715. [PubMed: 19555783]
4. Porter SE, Hanley EN. The musculoskeletal effects of smoking. Am. Acad. Orthop. Surg 2001;9:9–17.
5. Griffith JF, Yeung DK, Tsang PH, et al. Compromised bone marrow perfusion in osteoporosis. J. Bone Miner. Res 2008;23:1068–1075. [PubMed: 18302498]
6. Lee JH, Dyke JP, Ballon D, et al. Subchondral fluid dynamics in a model of osteoarthritis: use of dynamic contrast-enhanced magnetic resonance imaging. Osteoarthritis Cartilage 2009;17:1350–1355. [PubMed: 19409292]
7. Wehrli FW. Structural and functional assessment of trabecular and cortical bone by micro magnetic resonance imaging. J. Magn. Reson. Imaging 2007;25:390–409. [PubMed: 17260403]

8. Aaron RK, Dyke JP, Ciombor D. McK, et al. Perfusion abnormalities in subchondral bone associated with marrow edema, osteoarthritis, and avascular necrosis. Ann. N. Y. Acad. Sci 2007;1117:124–137. [PubMed: 18056039]
9. Tofts PS. Modeling tracer kinetics in dynamic Gd-DTPA MR imaging. J. Magn. Reson. Imaging 1997;7:91–101. [PubMed: 9039598]
10. Lee JH, Dyke JP, Ballon D, et al. Assessment of bone perfusion with contrast-enhanced magnetic resonance imaging. Orthop. Clin. North Am 2009;40:249–257. [PubMed: 19358910]
11. Wang YX, Griffith JF, Kwok AW, et al. Reduced bone perfusion in proximal femur of subjects with decreased bone mineral density preferentially affects the femoral neck. Bone 2009;45:711–715. [PubMed: 19555783]
12. Boraiah S, Dyke JP, Hettrich C, et al. Assessment of vascularity of the femoral head using gadolinium (Gd-DTPA)-enhanced magnetic resonance imaging: A Cadaver Study. J. Bone Joint Surg. [Br] 2009;91-B:131–137.
13. Van Dijke CF, Peterfy CG, Brasch RC, et al. MR Imaging of the arthritic rabbit knee joint using albumin-(Gd-DTPA)30 with correlation to histopathology. Magn. Reson. Imaging 1999;17:237–245. [PubMed: 10215479]
14. Tofts PS, Brix G, Buckley DL, et al. Estimating kinetic parameters from dynamic contrast-enhancedT1-weighted MRI of a diffusable tracer: standardized quantities and symbols. J. Magn. Reson. Imag 1999;10:223–232.
15. Patlak CS, Blasberg RG, Fenstermacher JD. Graphical evaluation of blood-to-brain transfer constants from multiple-time uptake data. J. Cereb. Blood Flow Metab 1983;3:1–7. [PubMed: 6822610]
16. Van Dijke CF, Kirk BA, Peterfy CG, et al. Arthritic temporomandibular joint: correlation of macromolecular contrast-enhanced MR imaging parameters and histopathologic findings. Radiology 1997;204:825–832. [PubMed: 9280267]
17. Nakamura H, Masuko H, Yudoh K, et al. Positron emission tomography with 18F-FDG in osteoarthritic knee. Osteoarthritis Cartilage 2007;15:673–681. [PubMed: 17336549]
18. Grant FD, Fahey FH, Packard AB, et al. Skeletal PET with 18F-fluoride: applying new technology to an old tracer. J. Nucl. Med 2008;49:68–78. [PubMed: 18077529]
19. Hawkins RA, Choi Y, Huang SC, et al. Evaluation of the skeletal kinetics of fluorine-18-fluoride ion with PET. J. Nucl. Med 1992;33:633–642. [PubMed: 1569473]
20. Frost ML, Blake GM, Crook PK, Marsden PC. Differences in regional bone perfusion and turnover between lumbar spine and distal humerus: ^{18}F-fluoride PET study of treatment-naïve and treated post-menopausal women. Bone 2009;45:942–948. [PubMed: 19660584]
21. Piert M, Winter E, Becker GA, et al. Allogenic bone graft viability after hip revision arthroplasty assessed by dynamic [18F]fluoride ion positron emission tomography. Eur. J. Nucl. Med 1999;26:615–624. [PubMed: 10369947]
22. Piert M, Zittel TT, Becker G, et al. Assessment of porcine bone metabolism by dynamic [18F]Fluoride ion PET: correlation with bone histomorphometry. J. Nucl. Med 2001;42:1091–1100. [PubMed: 11438633]

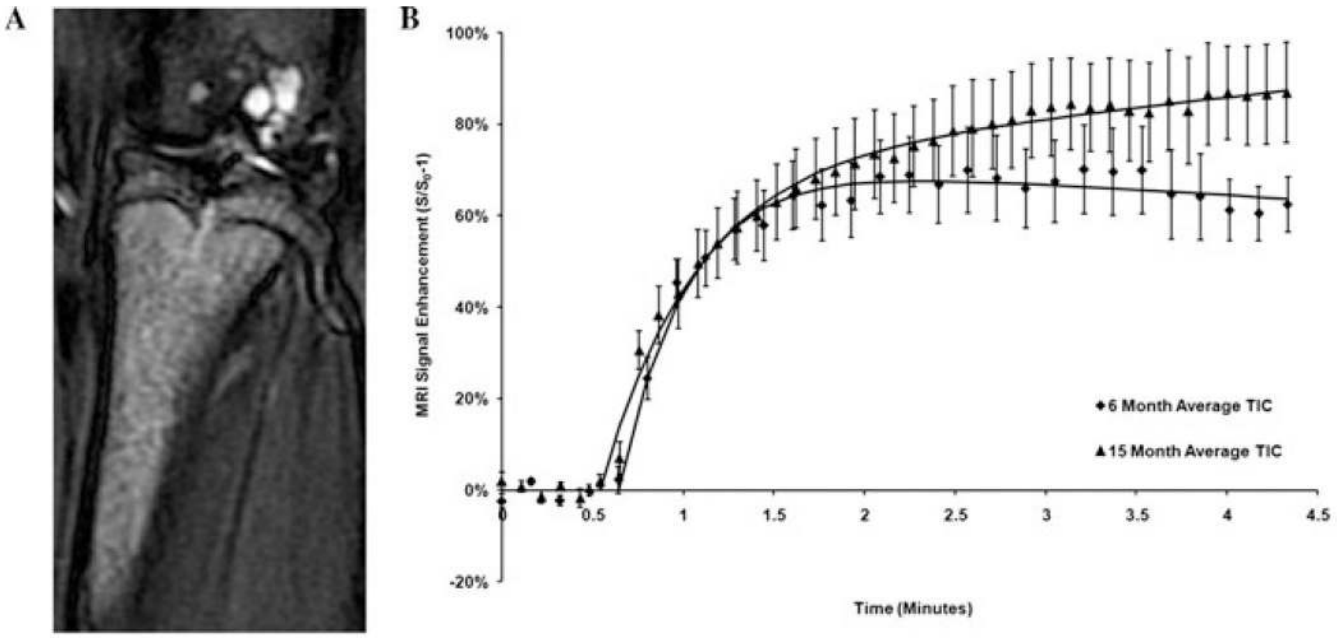

Figure 1.

(A) A coronal T_2-weighted MRI image of the tibial plateau acquired at 3.0 Tesla in a Dunkin-Hartley guinea pig model of osteoarthritis (OA). (B) Dynamic contrast-enhanced (DCE-MRI) time-intensity curves (TIC) taken in the medial tibial plateau are shown following administration of Gd-DTPA. Curves are averaged for animals ($n = 6$) of 6 months of age before morphologic changes of OA are apparent and for animals of 15 months of age with established changes of OA revealing diminished perfusion.

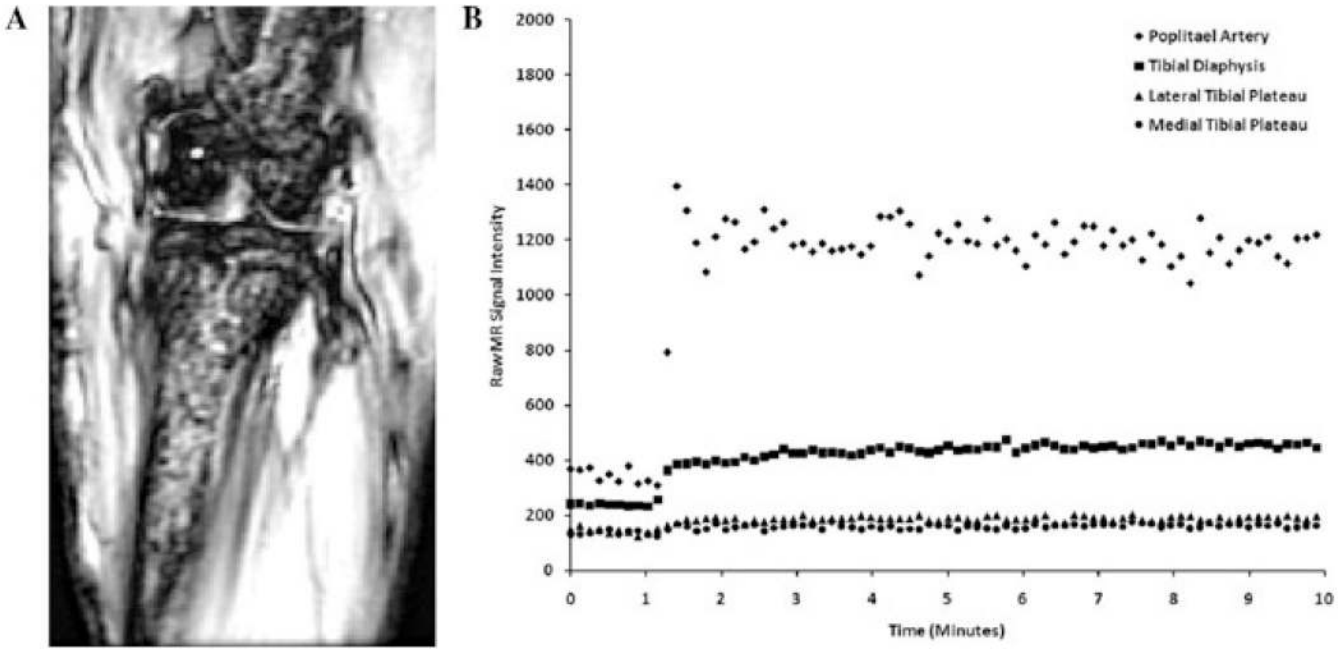

Figure 2.

(A) A time-averaged T_1-weighted image of the tibial plateau acquired at 3.0 Tesla in a Dunkin-Hartley guinea pig following injection of albumin-(Gd-DTPA)[30]. (B) Time intensity curves show constant uptake throughout the scan in the popliteal artery as well as various regions of bone.

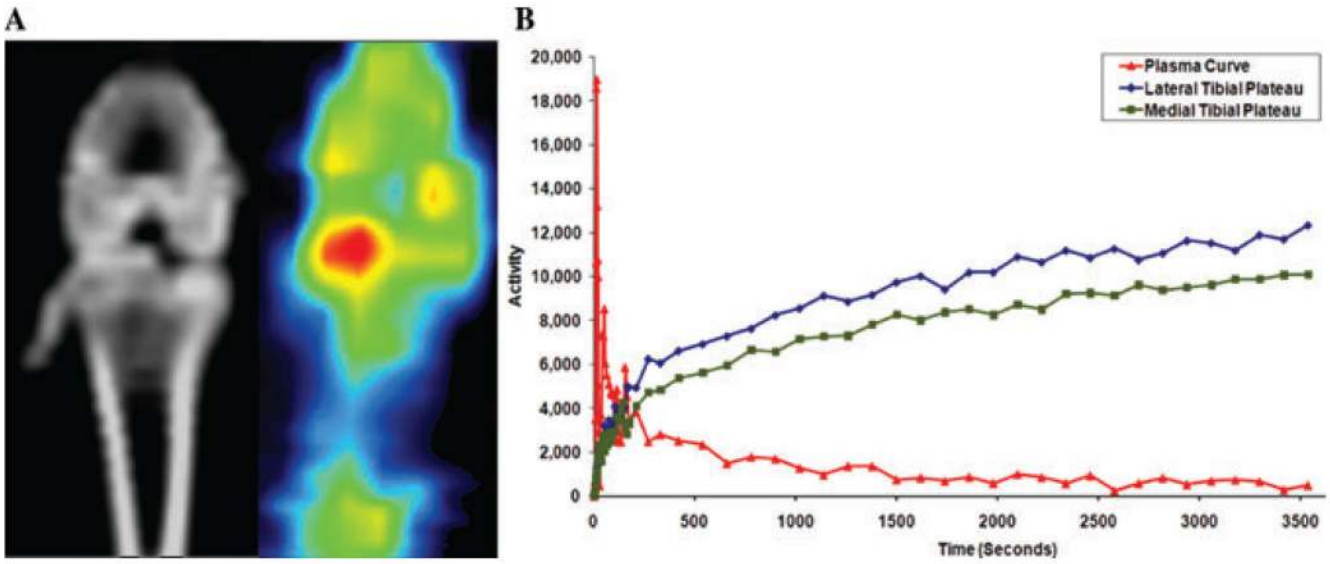

Figure 3.
(A) CT and ^{18}F-Fluoride PET images are shown of an 18-month-old Dunkin-Hartley guinea pig model of OA display differential PET uptake in the medial and lateral tibial plateaus. (B) The TAC is shown for regions of the tibial plateau as well as for the arterial input function that was used in pharmacokinetic and Patlak analysis.

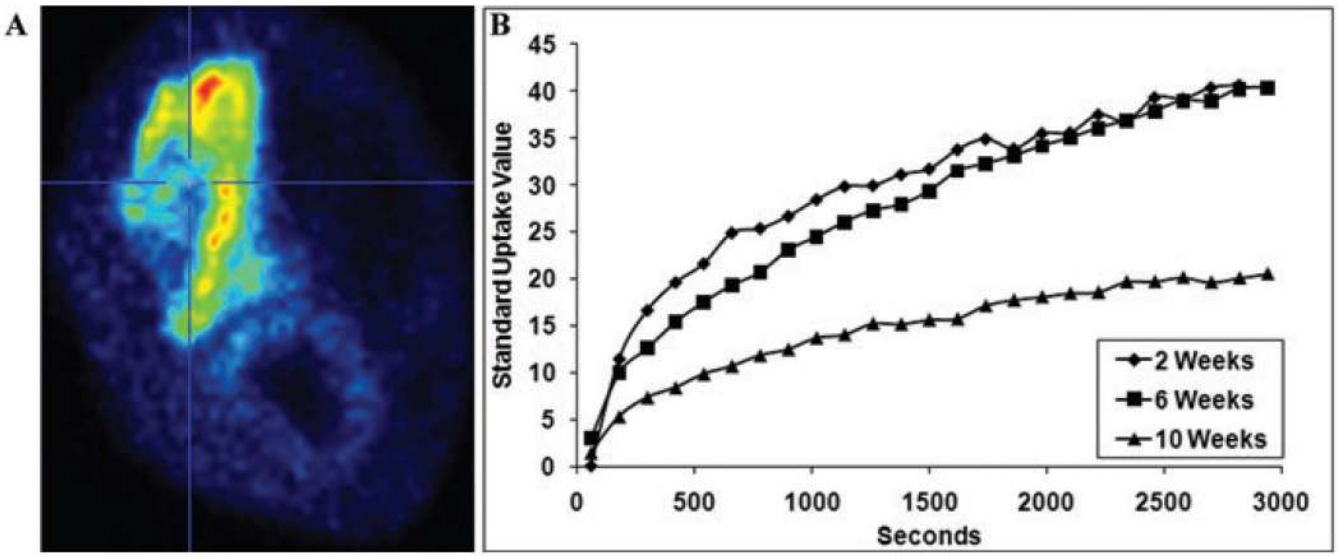

Figure 4.

(A) A static transaxial ^{18}F-Fluoride dynamic PET image in a fracture of the distal radius is shown. Increased uptake can be seen in the cortical region of the distal radius at 2 weeks following insult. Minimal uptake can also be seen in the adjacent ulna, although styloid fractures of the ulna require that the contralateral side also be imaged. Images were coregistered between serial time points and normalized to the standard uptake value. (B) An intensity contour map was used to focus on a region of interest on the cortical uptake at baseline that was then copied to the 1-month and 2-month time points. The subsequent time activity curves for this subject show a gradual decrease in ^{18}F-Fluoride uptake over the course of normal healing (courtesy of J.P. Dyke, M. Synan, S. Vallabhajosula, S. Goldsmith, O. Paul, J. Lane, and D. Lorich)